Coastal Engineering 165 (2021) 103852

Contents lists available at ScienceDirect

Coastal Engineering

journal homepage: http://www.elsevier.com/locate/coastaleng

Theoretical analysis of the laminar boundary layer beneath forward-leaning waves

Yiqin Xie [a,b], Jifu Zhou [a,b,*], Xu Wang [a], Jinlong Duan [a]

[a] Key Laboratory for Mechanics in Fluid Solid Coupling Systems, Institute of Mechanics, Chinese Academy of Sciences, Beijing, 100190, China
[b] School of Engineering Sciences, University of Chinese Academy of Sciences, Beijing, 100049, China

ARTICLE INFO

Keywords:
Forward-leaning waves
Near bed orbital velocity
Theoretical solution
Laminar boundary layer
Bottom shear stress

ABSTRACT

Wave-induced sediment transport is an important issue in coastal engineering. It is of fundamental significance to manifest the boundary layer behavior of nonlinear waves to accurately describe sediment transport in coastal areas, where wave forms are typically cnoidal or forward leaning rather than sinusoidal or symmetrical. In the present work, a novel expression of the near bed orbital velocity beneath forward-leaning waves is worked out. It is a series in which the coefficients are invariable for arbitrarily forward-leaning waves and just depend on the order of expansion. Based on this new expression, a theoretical solution of the laminar boundary layer beneath forward-leaning waves is derived by solving the governing equation via the method of variable separation. With this theoretical solution, it is convenient to acquire the velocity and shear stress (especially at the bottom) of the boundary layer beneath forward-leaning waves, which are different from those beneath sinusoidal waves as the degree of forward leaning increases. The phase lag between the bottom shear stress and the free-stream velocity is also analyzed, as well as the boundary layer thickness. In addition, the applicability of the present theory is discussed by comparing theoretical results with numerical results of different flow regimes.

1. Introduction

Wave-induced sediment transport is an important issue in coastal engineering. The flow characteristics, such as turbulence, velocity and bottom shear stress, in the boundary layer beneath waves are responsible for sediment suspension from the bed into the water. Therefore, it is a prerequisite to understand the behavior of the boundary layer flow beneath waves prior to addressing wave-induced sediment transport.

In the ocean, the nonlinearity of waves increases as the waves propagate towards the shore, thereby causing wave velocity and acceleration to become more and more asymmetrical, and the free surface is mostly in the form of a forward-leaning shape before breaking (Watanabe and Sato, 2004). Unlike those of linear or symmetrical waves, the profile, velocity and acceleration of forward-leaning waves are asymmetrical within one wave period, although the wave amplitudes are equal at wave crest and trough. Previously, most of the theoretical solutions for wave motion are obtained under the assumption of potential flow and linear waves or symmetrical waves. Thus, these theoretical solutions cannot be applied for nonlinear waves. In addition, it is necessary to investigate the boundary layer of waves from the level of mechanism, where the viscosity of water should be considered, in order to study wave-induced sediment transport thoroughly. Therefore, theoretical investigation of boundary layer flow beneath nonlinear or asymmetrical waves is of great practical implications for sediment transport in coastal areas, even if the flow is laminar.

According to wave theory of shallow water, the vertical velocity of water particles decreases as the depth increases, and the vertical velocity can be ignored when the water particles are located near the bottom. Thus, the flow of wave-induced boundary layer is almost same as that generated in the oscillatory boundary layer (the layer near a plate that oscillates horizontally in a quiescent water). This near bed oscillation is simply sinusoidal for linear waves and non-sinusoidal for nonlinear waves. Therefore, it is necessary to properly express the near bed orbital velocity of the oscillation motion of water so as to investigate the boundary layer beneath nonlinear waves. Correspondingly, related works have been reported since last century. Stokes (1847) first presented the skewed wave velocity prior to wave breaking. Larson (1996) used a velocity given by stream function theory as the near bed orbital velocity when investigating wave boundary layers. Drake and Calantoni (2001) considered a near bed orbital velocity in terms of a sine series as

* Corresponding author. Key Laboratory for Mechanics in Fluid Solid Coupling Systems, Institute of Mechanics, Chinese Academy of Sciences, Beijing, 100190, China.
E-mail address: zhoujf@imech.ac.cn (J. Zhou).

https://doi.org/10.1016/j.coastaleng.2021.103852
Received 27 February 2020; Received in revised form 10 November 2020; Accepted 10 January 2021
Available online 15 January 2021
0378-3839/

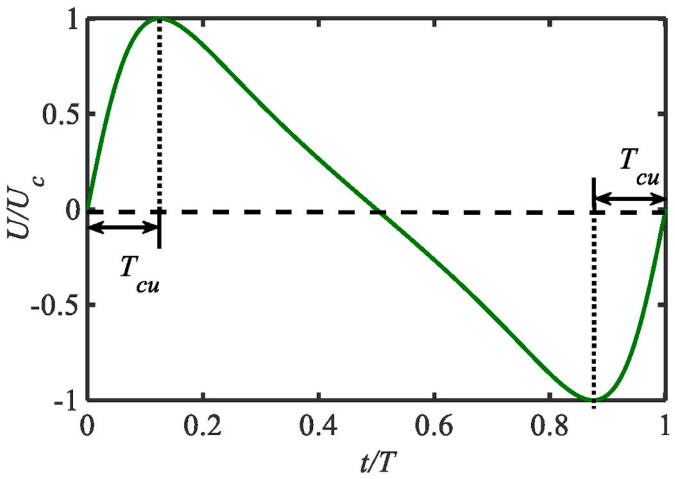

Fig. 1. Schematic diagram of free-stream velocity of forward-leaning waves.

being representative of a wide range of shoaling and broken waves. Similarly, van der A et al. (2011) also applied a sine series to conduct experimental investigation on the effects of acceleration asymmetry on the oscillatory boundary layer. Elfrink et al. (2006) proposed a method to express time varying near bed orbital velocity by using a set of simple sinusoidal functions for each segment between the maximum velocities and the zero crossings. Almost all these researches about the near bed orbital velocity induced by nonlinear waves are based on superposition of sinusoidal functions. However, this kind of expressions inevitably leads to velocity asymmetry, which has a large influence on the bottom shear stress. As a result, the near bed orbital velocity induced by a forward-leaning wave with equal velocity amplitudes at its crest and trough cannot be accurately described by these expressions. To alleviate this problem, Silva et al. (2007) proposed a formula for the near bed orbital velocity of forward-leaning waves, which is derived from the acceleration time series that is just similar to the velocity profile of a first-order cnoidal wave. Then, Abreu et al. (2010) provided an analytical expression for arbitrarily varying free-stream velocity, which is a proper choice for discussing forward-leaning waves.

Once the near bed orbital velocity is determined, model can be developed to analyze the characteristics of the boundary layer beneath nonlinear waves, such as the velocity and shear stress. Kondo (1956) derived an analytical solution for the laminar boundary layer of arbitrarily varying free-stream velocity by means of Laplace transformation (Nadaoka et al., 1996), which is given in an integral form and is inconvenient to be used. Tanaka et al. (1998) derived a Fourier series expansion for the solution of the laminar boundary layer beneath cnoidal waves, which are different from forward-leaning waves in their processes of free surface elevation, velocity and acceleration. Foster et al. (1999) also gave an analytical solution for the bottom boundary layer under an arbitrarily varying free-stream wave, but the parameters in it are difficult to verify. There are also some models for calculating the bottom shear stress by means of empirical analysis or analogy approach. Nielsen (2002) and Nielsen and Callaghan (2003) suggested a method for calculating the bottom shear stress of laminar flow beneath waves of arbitrary shape and extended it to turbulent flows by analogy to sinusoidal waves. Suntoyo et al. (2008) also presented a calculation method for bottom shear stress of turbulent boundary layers beneath forward-leaning waves, which is an analogy of the solution for harmonic laminar boundary layer flows to turbulent flows.

Except for a few theoretical researches as stated above, most of these previous studies for the boundary layers of forward-leaning waves are performed by numerical or experimental simulations. For example, Hsu and Hanes (2004) analyzed the effects of wave shape of forward-leaning waves on sediment transport by a two-phase model, in which a 4-term sine series is used as wave forcing. Scandura et al. (2016) discussed the characteristics of bottom shear stress and velocity of acceleration-skewed oscillating flows by direct numerical simulations. Watanabe and Sato (2004) proposed a formula of sheet-flow transport rate for forward-leaning waves by the experiment of acceleration-asymmetric oscillatory flow. Yuan and Madsen (2014) studied turbulent oscillatory boundary layers induced by forward-leaning waves in an oscillating wave tunnel. They generated forward-leaning waves by a full-scale experiment to investigate the acceleration-skewness-induced net sediment transport rate, in which the free-stream velocity is given by the superposition of two harmonics. These experimental and numerical investigations can deal with turbulent boundary layer flows. However, these methods are more time-consuming compared with the theoretical method. In addition, it is generally more effective and explicit to delineate the law in a theoretical way. Therefore, it is important to develop theoretical model for the boundary layer beneath forward-leaning waves. Even if the theory is developed for laminar flows, it may be extended to turbulent flows as was done by Nielsen (2002), Nielsen and Callaghan (2003) and Suntoyo et al. (2008).

The objective of the present work is to derive an analytical solution for laminar boundary layer beneath forward-leaning waves. To begin with, a novel expression of the near bed orbital velocity beneath forward-leaning waves is worked out, which is further used as the boundary condition of the governing equation of the boundary layer beneath the forward-leaning waves. Then, the analytical solution of the laminar boundary layer beneath forward-leaning waves is derived by solving the governing equation via the method of variable separation. The coefficients of the series are invariable for arbitrarily forward-leaning waves. Consequently, the fundamental characteristics of the laminar boundary layer beneath forward-leaning waves are thoroughly studied and understood based on the analytical solution obtained here. Finally, the applicability of the present theory is discussed by quantitatively analyzing errors of velocity and bottom shear stress between the results calculated by the present theory and the numerical results of different flow regimes.

2. Theory and numerical model description

2.1. Theory

As stated in the introduction, the wave-induced boundary layer can be considered as the oscillatory boundary layer. For incompressible fluid, the boundary layer of laminar flow can be described by

$$\frac{\partial u}{\partial t}=\nu\frac{\partial^2 u}{\partial z^2}, \tag{1}$$

where u is the horizontal velocity, ν the kinematic viscosity of the fluid, t the time and z the vertical coordinate.

Since only the motion of water near the boundary is considered, the boundary layer of the oscillatory flow induced by waves can be equivalent to the boundary layer caused by an oscillating plate. So the boundary conditions are given by

$$u|_{z\to\infty}=U(t),\quad u|_{z=0}=0\,, \tag{2}$$

where $U(t)$ is the free-stream velocity outside the boundary layer, namely the near bed orbital velocity induced by waves. For the purpose of investigation of the boundary layer beneath forward leaning waves, the near bed orbital velocity can be expressed as follows (Abreu et al., 2010)

$$U(t)=U_c\sqrt{1-r^2}\ \frac{\sin\omega t}{1-r\cos\omega t}, \tag{3}$$

where U_c is the maximum velocity at the wave crest, ω the angular frequency, and r the waveform parameter$(0\le r<1)$, which describes the wave acceleration asymmetry. The waveform parameter r depends

Table 1
Value of $a_{k,m}$.

k \ m	1	2	3	4	5	6	7	8	9	…
0	1	-	-	-	-	-	-	-	-	…
1	0	1	-	-	-	-	-	-	-	…
2	1	0	1	-	-	-	-	-	-	…
3	0	2	0	1	-	-	-	-	-	…
4	2	0	3	0	1	-	-	-	-	…
5	0	5	0	4	0	1	-	-	-	…
6	5	0	9	0	5	0	1	-	-	…
7	0	14	0	14	0	6	0	1	-	…
8	14	0	28	0	20	0	7	0	1	…
⋮	⋮	⋮	⋮	⋮	⋮	⋮	⋮	⋮	⋮	

on the degree of forward leaning β, which is defined as follows (Watanabe and Sato, 2004)

$$\beta = 1 - \frac{2T_{cu}}{T}, \tag{4}$$

where T represents the wave period, T_{cu} the time for the velocity to increase from zero to the maximum as shown in Fig. 1. According to this definition of β, r can be expressed as (Abreu et al., 2010)

$$r = -\cos(\pi\beta). \tag{5}$$

It is obvious that β equals to 0.5 for sinusoidal waves. Then, r equals to 0 and Eq. (3) reduces to a harmonic function. As r closes to 0.8 for broken waves (Silva et al., 2007), β is generally less than 0.8.

It should be stressed that Eq. (3) is a particular solution of the analytical formulation of Abreu et al. (2010) for pure forward-leaning waves and can represent the near bed orbital velocities of forward-leaning waves in nature. Abreu et al. (2010) proposed the formulation for the orbital velocity of shallow water waves with both velocity and acceleration asymmetries and concluded that their analytical formulation can represent the time varying near bed orbital velocities measured in the near shore region and under breaking and non-breaking waves by validating against field and laboratory experiment data. Therefore, it is evident that Eq. (3) can describe the near bed orbital velocities of forward-leaning waves in nature.

To solve the problem analytically, Eq. (3) is expanded into a Taylor series, which reads

$$\frac{\sin\omega t}{1 - r\cos\omega t} = \sin\omega t + (r\cos\omega t)\sin\omega t + (r\cos\omega t)^2 \sin\omega t \cdots + (r\cos\omega t)^k \sin\omega t + \cdots. \tag{6}$$

In Eq. (6), the trigonometric relation can be expressed as

$$(r\cos\omega t)^k \sin\omega t = \left(\frac{r}{2}\right)^k \left[\sum_{m=1}^{k+1} a_{k,m} \sin(m\omega t)\right], \tag{7}$$

where the coefficients $a_{k,m}$ satisfy the rules as follows

$$\begin{cases} a_{0,1} = 1 \\ a_{1,1} = 0 \\ a_{k,m} = 0, m > k+1 \\ a_{k,m} = 1, m = k+1 \\ a_{k,m} = \sum_{n=1}^{m} a_{k-n,m-n+2}, \quad k \geq 2, 2 \leq m < k+1 \\ a_{k,m} = a_{k-1,m+1}, \quad m = 1, k \geq 2 \end{cases}, \tag{8}$$

It is nicely noted that these coefficients are invariable for arbitrarily forward-leaning waves and just depend on the order of expansion. All the values of $a_{k,m}$ can be intuitively displayed by a lower triangular matrix as shown in Table 1. The coefficients on the diagonal are equal to 1 and those on the dashed lines are 0. The red and black arrows demonstrate the law of the values of the coefficients, similar to the law of Yang Hui's Triangle to some extent.

Substituting Eq. (7) into Eq. (6) and considering Eq. (3), the following series expansion can be acquired

$$U(t) = U_c \sum_{m=1}^{N} A_m \sin(m\omega t), \tag{9}$$

where the coefficients are

$$A_m = \sqrt{1 - r^2} \sum_{k=m-1}^{N-1} a_{k,m} \left(\frac{r}{2}\right)^k. \tag{10}$$

Based on Eq. (9) and applying the method of variable separation to Eqs. (1) and (2), a solution for velocity and shear stress (especially at the bottom) in the laminar boundary layer can be obtained as follows

$$u(z,t) = \sum_{m=1}^{N} A_m \left\{ U_c \sin(m\omega t) - e^{-\frac{z}{\sqrt{2\nu/(m\omega)}}} \cdot U_c \sin\left(m\omega t - \frac{z}{\sqrt{2\nu/(m\omega)}}\right) \right\}, \tag{11}$$

and

$$\tau^*(z,t) = \frac{\tau}{\rho U_c \sqrt{\omega\nu}} = \sum_{m=1}^{N} A_m \sqrt{m} \cdot e^{-\frac{z}{\sqrt{2\nu/(m\omega)}}} \sin\left(m\omega t + \frac{\pi}{4} - \frac{z}{\sqrt{2\nu/(m\omega)}}\right), \tag{12}$$

where τ is the shear stress and τ^* is the dimensionless shear stress. Thus, the bottom shear stress reads

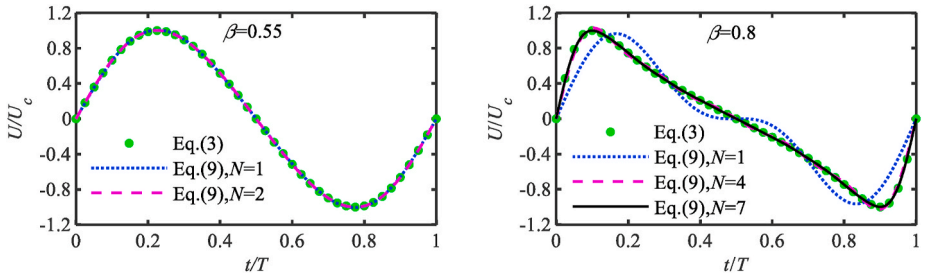

Fig. 2. Near bed orbital velocity process expressed by Eq. (3) and Eq. (9) with different number of the series terms. Left for $\beta = 0.55$ and right for $\beta = 0.8$.

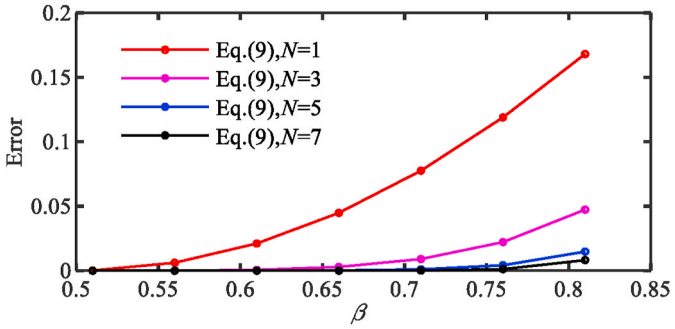

Fig. 3. Errors between series expression (Eq. (9)) and exact solution (Eq. (3)).

$$\tau_0^*(t) = \frac{\tau_0}{\rho U_c \sqrt{\omega\nu}} = \sum_{m=1}^{N} A_m \sqrt{m} \cdot \sin\left(m\omega t + \frac{\pi}{4}\right), \tag{13}$$

where τ_0 is the bottom shear stress and τ_0^* is the dimensionless bottom shear stress.

2.2. Numerical model

A numerical model has been developed to simulate the wave boundary layer flow of different flow regimes. The wave boundary layer flow is modeled by oscillating an infinite plate in a quiescent water with the near bed orbital velocity induced by waves. In the model, large eddy simulation is used to solve the spatially filtered time-dependent 3-D Navier–Stokes equations with Smagorinsky subgrid model (Lohman et al., 2006).

The boundary conditions in the streamwise and spanwise directions are periodic boundary conditions since turbulence in these directions is homogeneous. In the vertical direction, a non-slip boundary condition is enforced at the bottom wall, and a free-slip condition is used at the top boundary, as expressed by Eq. (2).

Uniform grids are adopted in the streamwise and spanwise directions, and non-uniform staggered grids are used in the vertical direction. The resolution of the near bed grids is fine enough for wall turbulence modeling. The mixed spectral and finite difference algorithm is used in the simulations. Derivatives in the streamwise and spanwise directions are treated with a pseudo-spectral method. Derivatives in the vertical direction are computed with second-order center difference in the vertical staggered grids. The second-order Adams-Bashforth method is adopted for time-marching (Zhang et al., 2005; Li et al., 2016).

The model has been verified based on the experimental data of the laminar flow ($Re_\delta = 392, As = 0.69$), intermittent turbulent flow ($Re_\delta = 936$, $As = 0.62$), and fully turbulent flow ($Re_\delta = 3464$, $As = 0.5$) beneath cnoidal waves, where the flow regime is divided by the boundary layer Reynolds number $Re_\delta = U_c\delta/\nu$ and As is the degree of asymmetry, referring to Tanaka et al. (1998) for details. The experimental data are from the literature of Sana et al. (2006) and Tanaka et al. (1998). Refer to Li et al. (2016) for details of the validation of this model.

This numerical model is used here to simulate the velocity and bottom shear stress of forward-leaning waves and to investigate the applicability of Eqs. (11) and (13).

3. Discussion of near bed orbital velocity

As already stated above, the properties of the boundary layer induced by a forward-leaning wave can be obtained analytically when Eq. (9) is taken as the free stream boundary condition of Eq. (1). Tanaka et al. (1998) pointed out that the bottom shear stress is very sensitive to the free stream boundary condition, so the agreement between Eq. (9) and Eq. (3), the exact expression of the near bed orbital velocity beneath forward-leaning waves, has a great effect on the bottom shear stress. Therefore, it is very important to address the accuracy of Eq. (9) to model Eq. (3).

3.1. Appropriateness of Eq. (9) to represent Eq. (3)

The appropriateness of Eq. (9) to represent Eq. (3) is examined as shown in Fig. 2, which demonstrates the performance of Eq. (9) with different N to reproduce the exact processes of the near bed orbital velocity induced by forward-leaning waves for $\beta = 0.55$ and $\beta = 0.8$. It should be noted that $\beta = 0.55$ and $\beta = 0.8$ respectively represent the two extreme cases of forward-leaning waves. The former case is close to the sinusoidal waves and the latter one represents the forward-leaning wave that is nearly broken (Silva et al., 2007).

As shown in Fig. 2, the results obtained from Eq. (9) is accurate enough for $\beta = 0.55$ when $N = 1$, and for$\beta = 0.8$ when $N = 4$. In order to analyze quantitatively the truncation error of Eq. (9), the periodic averaged Error is introduced (Tanaka et al., 1998)

$$\text{Error} = \left[\sum_{i=1}^{M}\left(\frac{U_{i(ex)}}{U_c} - \frac{U_{i(ap)}}{U_c}\right)^2 \Big/ M\right]^{1/2}, \tag{14}$$

where the i is the time index in a wave cycle, and the subscripts (ex) and (ap) denote the exact expression (Eq. (3)) and the series expansion (Eq. (9)), respectively. Fig. 3 presents the errors between the series expansion and the exact solution, where M is equal to 2000. It is seen that the errors decrease with an increase in N and increase with an increase in β. When $N = 7$, the error is less than 0.0058 for $\beta < 0.8$. As a matter of fact, the velocity-leaning index of non-breaking forward-leaning waves is generally less than 0.8 as already stated in Section 2.1. Therefore, it is accurate enough to use Eq. (9) instead of Eq. (3) to delineate the boundary layer behavior beneath forward-leaning waves.

3.2. Comparison between Eq. (9) and other models

Apart from the error analysis above, results from Eq. (9) are further compared with those based on other similar models of asymmetric orbital velocity in this section.

Based on the error analysis in Section 3.1, it can be concluded that Eq. (9) can also represent the near bed orbital velocities of the real waves accurately instead of Eq. (3). In order to further examine the accuracy of

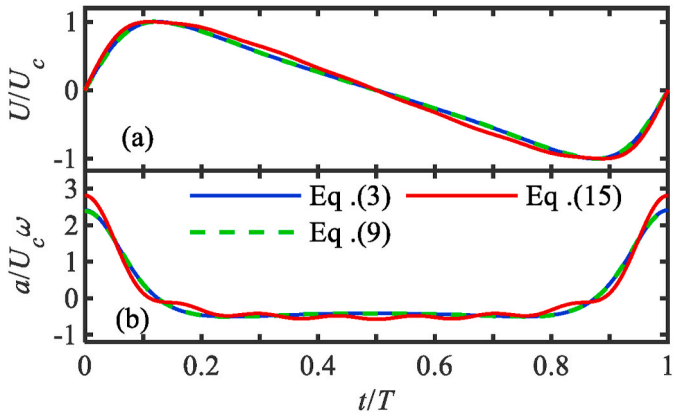

Fig. 4. Comparison of free-stream velocity and acceleration time series computed by Eqs. (3), (9) and (15) for $N = 7$.

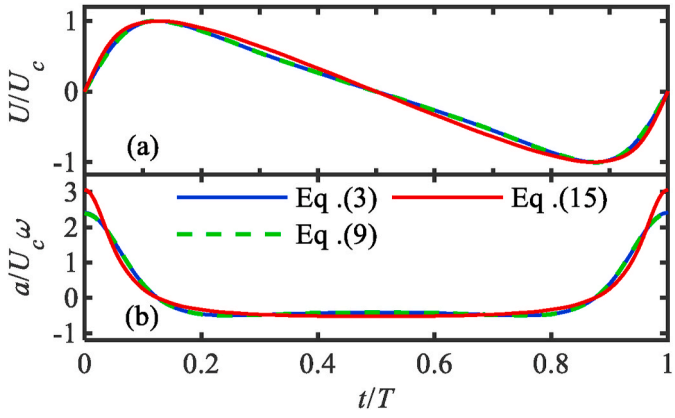

Fig. 5. Comparison of free-stream velocity and acceleration time series computed by Eqs. (3), (9) and (15) for $N = 20$.

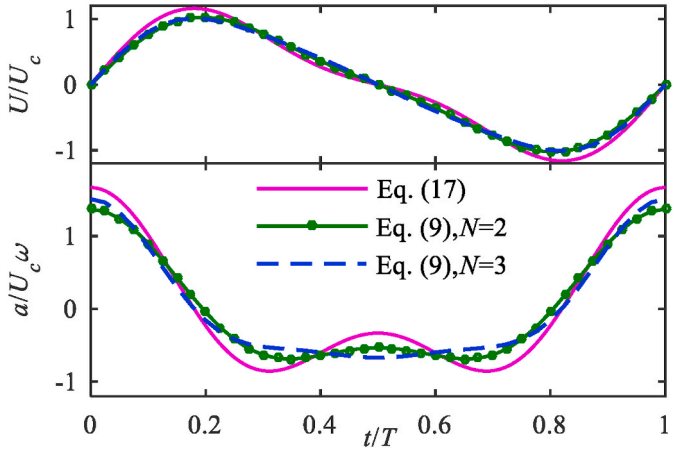

Fig. 6. Comparison of near bed orbital velocity and acceleration time series computed by Eqs. (9) and (17).

Eq. (9), the comparisons between Eq. (9) and other models are then conducted.

As stated, Eq. (9) is equivalent to Eq. (3). Since Eq. (3) has been proved available to describe the pure forward-leaning waves more appropriately based on the comparison with the other models proposed by Drake and Calantoni (2001), Elfrink et al. (2006) and Silva et al. (2007) as conducted by Abreu et al. (2010), Eq. (9) also has the same advantages as Eq. (3). Therefore, comparison between Eq. (9) and these previous models is not performed here again. However, the expressions of the near bed orbital velocity beneath forward-leaning waves presented by van der A et al. (2011) and Wang and Yuan (2020) are chosen here. Then the superiority of Eq. (9) is examined by comparing with these two formulations.

van der A et al. (2011) employed a total of six sinusoidal flows as the free-stream velocity to conduct experimental investigation of the effects of acceleration asymmetry on the oscillatory boundary layer, which is given by

$$U(t) = \alpha U_c \sum_{i=1}^{6} \frac{(2\xi - 1)^{i-1}}{i} \sin(i\omega t), \tag{15}$$

where α is a multiplier that lets the maximum value of $U(t)$ equal to U_c; ξ is a parameter to describe the acceleration skewness defined as

$$\xi = \frac{a_{max}}{a_{max} - a_{min}}, \tag{16}$$

where a is the acceleration of free-stream velocity.

Now, the summation of N-term sinusoidal flows of Eq. (15) is analyzed. By computing the forward-leaning degree from Eqs. (9) and (15), it is found that $N = 7$ is enough to get a stable and sufficient accurate waveform by Eq. (9) for most of β, whereas the value of N should be larger than 20 by Eq. (15). Fig. 4 (a) and 5(a) represent the dimensionless $U(t)$ obtained from Eqs. (3), Eq. (9) and Eq. (15) respectively, for $\beta = 0.75$. The corresponding dimensionless $a(t)$, which can be readily obtained by dU/dt, are displayed in Figs. 4(b) and 5(b), respectively. It is evident that both Eqs. (9) and (15) present an oscillatory acceleration time series when $N = 7$, but Eq. (15) presents unstable results with small fluctuations. When $N = 20$, the results calculated by both Eqs. (9) and (15) are stable. Here, the small fluctuations shown in Fig. 4(b) are induced by the truncation of Eq. (15) and these fluctuations are definitely not the real case of acceleration in nature. Both Abreu et al. (2010) and Ruessink et al. (2009) considered that these fluctuations should disappear. They took this disappearance as a rule to judge whether a theoretical expression of the orbital velocity is good or bad. The results for $a(t)$ demonstrate that 18 terms are required for Eq. (15) to make these fluctuations disappear, while only 5 terms are enough for Eq. (9). From this point of view, it can be concluded that it is more accurate to use Eq. (9) rather than Eq. (15) to describe the near bed orbital velocity beneath forward-leaning waves.

Wang and Yuan (2020) adopted a simple approximation for the free-stream velocity of forward-leaning waves, which reads

$$U(t) = U_c \sin(\omega t) + \zeta U_c \sin(2\omega t), \tag{17}$$

where ζ is a coefficient. The coefficient can adjust the degree of forward leaning of velocity. For instance, when $\zeta = 1/3$, the degree of forward leaning can be calculated by Eq. (17), equal to 0.638. Fig. 6 presents the time series of orbital velocity and acceleration calculated using Eq. (17) with $\zeta = 1/3$. Also shown in Fig. 6 for comparison are the time series of orbital velocity and the corresponding acceleration calculated using Eq. (9) with $N = 2$ and $N = 3$. The degree of forward leaning calculated by Eq. (9) is equal to that obtained by Eq. (17). It is evident from Fig. 6 that the acceleration time series of Eq. (17) near the zero down-crossing of velocity is more concave or convex than that of Eq. (9). According to the consideration of Abreu et al. (2010) and Ruessink et al. (2009) as stated above, Eq. (9) is obviously more reasonable than Eq. (17) to describe the near bed orbital velocity beneath forward-leaning waves. In addition, Eq. (9) with $N = 3$ presents much better results as shown in Fig. 6, where the velocity time series of $N = 3$ almost totally overlaps that of $N = 2$ and the acceleration time series of $N = 3$ is almost same as the theoretical one, i.e. a cnoidal wave shape.

The forgoing analyses demonstrate that Eq. (9) can describe the near bed orbital velocity beneath forward-leaning waves with enough

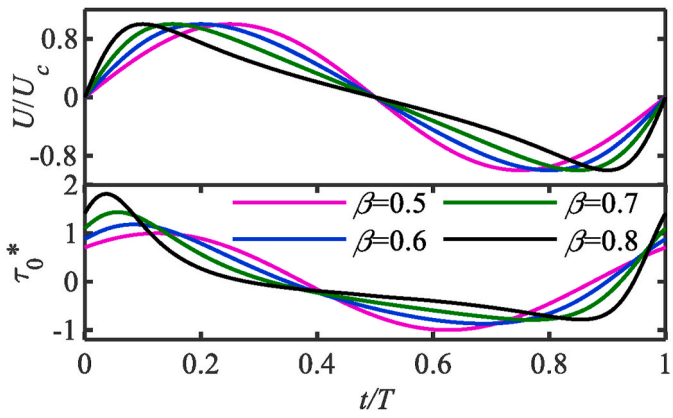

Fig. 7. Periodic variation of velocity (upper) and bottom shear stress (below) for different β.

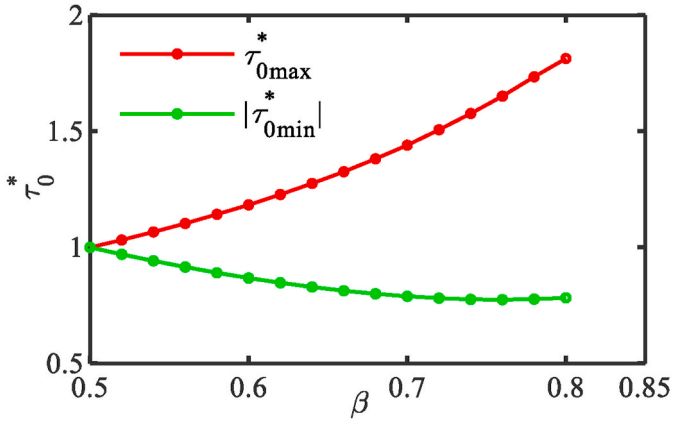

Fig. 8. The change of maximum and minimum bottom shear stress with β.

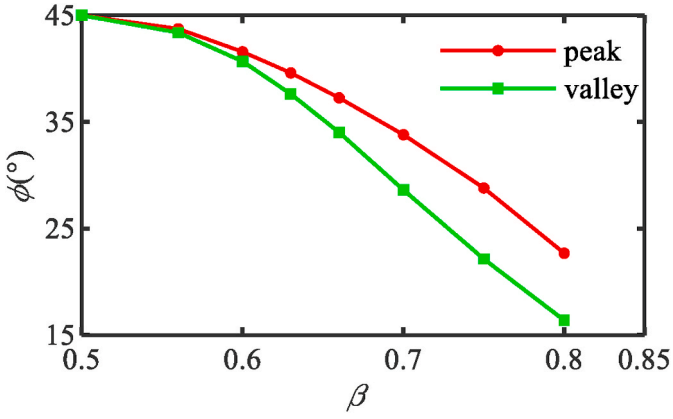

Fig. 9. The change of phase lag between free-stream velocity and bottom shear stress with β.

accuracy. By using Eq. (9) instead of Eq. (3) as the boundary condition of Eq. (1), one can conveniently obtain the analytical solution of the laminar boundary layer beneath forward-leaning waves.

4. Results of boundary layer solution and discussion

4.1. Velocity, bottom shear stress and boundary layer thickness

The theoretical results displayed hereafter for the velocity, bottom shear stress and boundary layer thickness are acquired by 10-term series of Eqs. (11) and (13), namely $N = 10$, to achieve sufficient accuracy for a wide range of waves from sinusoidal waves to near breaking waves ($\beta =$ 0.5–0.8). The periodic variation of bottom shear stress and the velocity for different β are plotted in Fig. 7. As Fig. 7 shows, the nonlinearity of the forward-leaning wave gets stronger and the waveform of the velocity process becomes steeper as β increases. The bottom shear stress follows the same rule, as shown in the lower panel of Fig. 7. Fig. 8 demonstrates the maximum and minimum bottom shear stress. The maximum and minimum bottom shear stress grow and decrease respectively with β, and the changing rate of the maximum is larger than that of the minimum. Fig. 9 presents the phase lag between the free-stream velocity and bottom shear stress. It can be seen that the phase lag decreases obviously from 45° for the sinusoidal wave with increasing β. And the phase lag at the crest is larger than that at the trough because of the acceleration asymmetry.

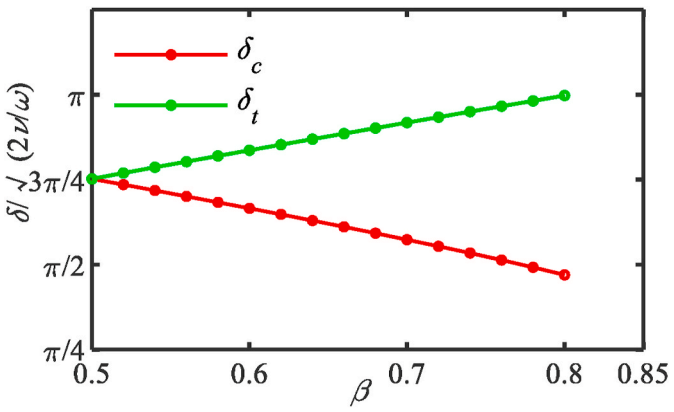

Fig. 10. The change of boundary layer thickness with β.

The dimensionless boundary layer thickness, which is normalized by the Stokes layer thickness $\delta = \sqrt{\frac{2\nu}{\omega}}$, is plotted in Fig. 10, where δ_c and δ_t are the boundary layer thickness at the wave crest and trough as defined in Jensen et al. (1989). δ_c and δ_t, respectively, decreases and increases almost linearly as β increases. Both δ_c and δ_t approach to $\frac{3\pi}{4}$, the counterpart values of sinusoidal waves (Jensen et al., 1989; Tanaka et al., 1998) when β decreases to 0.5. In addition, δ_c is always smaller than δ_t because of the shorter time for the increase of velocity to the maximum at crest than that at the trough.

4.2. Comparison with numerical results

Now let us discuss the applicability of Eqs (11) and (13) by comparing the theoretical results with numerical results obtained based on the numerical model described in Section 2. The numerical simulations are carried out for different flow regimes. The flow regime is divided into four stages based on the Reynolds number according to Jensen et al. (1989): laminar flow ($Re_\delta \leq 100$), disturbing laminar flow ($100 < Re_\delta \leq 550$), intermittent turbulent flow ($550 < Re_\delta \leq 3500$), and fully developed turbulence ($Re_\delta > 3500$).

4.2.1. Bottom shear stress

The left panels in Figs. 11 and 12 show the theoretical (dots calculated by Eq. (13)) and numerical (curves) periodic variation of dimensionless bottom shear stress at different Reynolds number for $\beta = 0.55$ and $\beta = 0.8$, respectively. The right panels are enlargements of the pink rectangles in the left panels with the curves for Re_δ over 1500 omitted.

As the left panel of Fig. 11 shows, the bottom shear stress increases with Re_δ. In particular, the increase is notable in the flow regime of fully developed turbulence. The theoretical results of dimensionless bottom shear stress show a perfect agreement with the numerical calculations

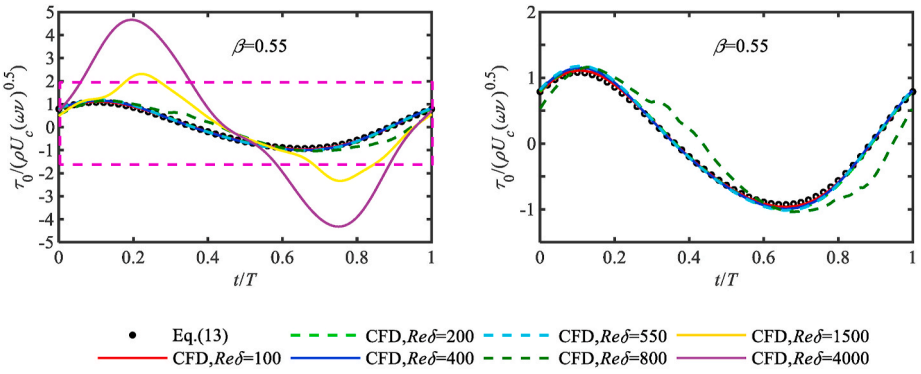

Fig. 11. The periodic variation of bottom shear stress for $\beta = 0.55$. The right panel is enlargement of the pink rectangle in the left panel with the curves for Re_δ over 1500 omitted. (For interpretation of the references to color in this figure legend, the reader is referred to the Web version of this article.)

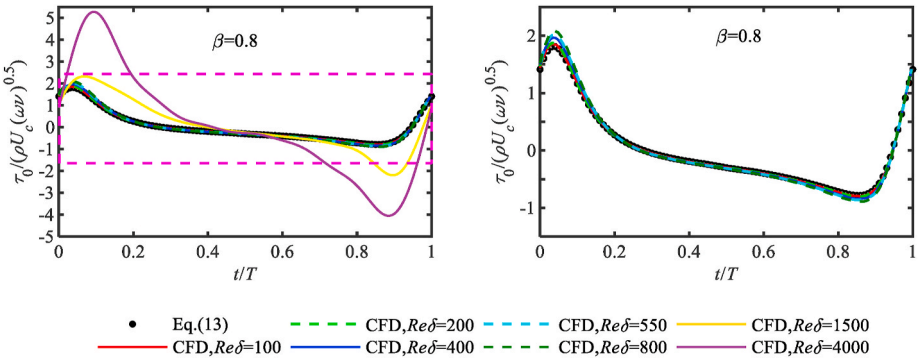

Fig. 12. The periodic variation of bottom shear stress for $\beta = 0.8$. The right panel is enlargement of the pink rectangle in the left panel with the curves for Re_δ over 1500 omitted. (For interpretation of the references to color in this figure legend, the reader is referred to the Web version of this article.)

Table 2
Periodic averaged error of bottom shear stress.

	$Re_\delta = 100$	$Re_\delta = 200$	$Re_\delta = 400$	$Re_\delta = 550$	$Re_\delta = 800$	$Re_\delta = 1500$	$Re_\delta = 4000$
$\beta = 0.55$	0.027	0.024	0.047	0.063	0.29	0.91	2.28
$\beta = 0.8$	0.015	0.020	0.055	0.076	0.11	0.69	1.90

Table 3
Maximum error of bottom shear stress.

	$Re_\delta = 100$	$Re_\delta = 200$	$Re_\delta = 400$	$Re_\delta = 550$	$Re_\delta = 800$	$Re_\delta = 1500$	$Re_\delta = 4000$
$\beta = 0.55$	0.042	0.040	0.078	0.11	0.57	1.60	3.82
$\beta = 0.8$	0.057	0.070	0.15	0.20	0.27	1.56	4.11

Table 4
Distribution of error for $\beta = 0.55$ (unit: %).

	≤0.01	>0.01 ≤0.05	>0.05 ≤0.1	>0.1 ≤0.2	>0.2 ≤0.5	>0.5
$Re_\delta = 100$	28.8	71.2	0	0	0	0
$Re_\delta = 200$	25.7	74.3	0	0	0	0
$Re_\delta = 400$	15.1	50.1	34.8	0	0	0
$Re_\delta = 550$	10.1	43.2	40.9	5.8	0	0
$Re_\delta = 800$	2.0	8.1	10.3	28.9	44.2	6.5
$Re_\delta = 1500$	1.3	4.8	5.3	10.0	22.8	55.8
$Re_\delta = 4000$	0.5	1.7	2.3	4.8	11.7	79.0

Table 5
Distribution of error for $\beta = 0.8$ (unit: %).

	≤0.01	>0.01 ≤0.05	>0.05 ≤0.1	>0.1 ≤0.2	>0.2 ≤0.5	>0.5
$Re_\delta = 100$	75.5	21.8	2.7	0	0	0
$Re_\delta = 200$	52.2	42.5	5.3	0	0	0
$Re_\delta = 400$	10.8	67.7	13.1	8.4	0	0
$Re_\delta = 550$	5.8	62.7	20.9	10.6	0	0
$Re_\delta = 800$	3.2	57.2	22.2	10.5	6.9	0
$Re_\delta = 1500$	2.1	10.9	12.1	14.1	19.4	41.4
$Re_\delta = 4000$	1.0	9.3	3.3	5.4	15.5	65.5

when $Re_\delta \leq 200$. In addition, the theoretical results agree with the numerical results very well when $200 < Re_\delta \leq 550$. Even if $Re_\delta = 800$, the theory can roughly predict the numerical results with reasonable discrepancy near the maximum velocity under wave crest and the minimum under wave trough, which is mainly attributed to stronger turbulence. A similar conclusion can be drawn from Fig. 12 for $\beta = 0.8$, although the difference between the theoretical and numerical results near the wave crest is more evident than compared with that in Fig. 11.

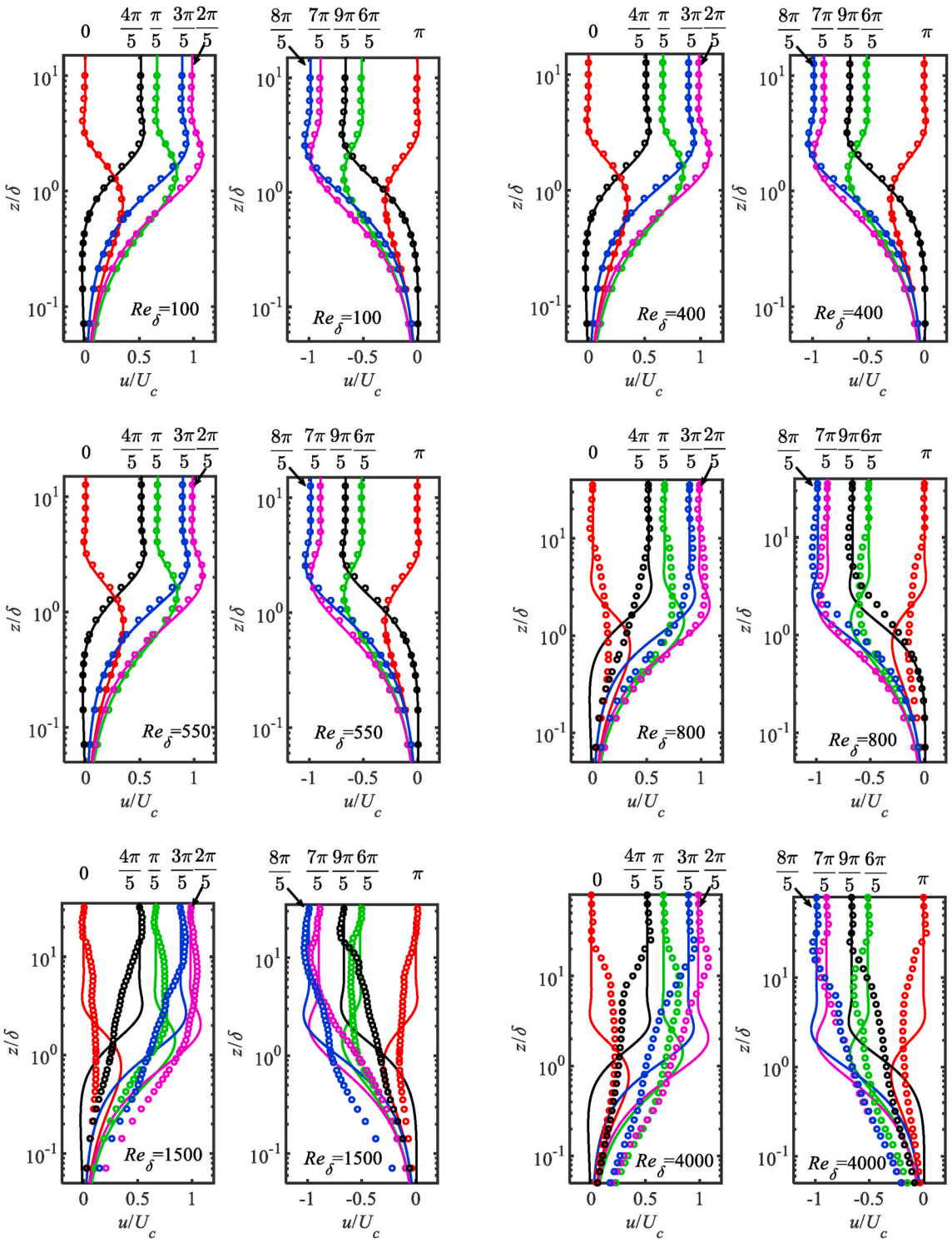

Fig. 13. Comparison between theoretical and numerical velocity profiles for $\beta = 0.55$. The lines and circles show the theoretical results of Eq. (11) and the numerical results, respectively. Different colors represent different phases. (For interpretation of the references to color in this figure legend, the reader is referred to the Web version of this article.)

To further make quantitative consideration on the applicability of Eq. (13), the periodic averaged error and the maximum error between calculations from Eq. (13) and the numerical results are computed. The periodic averaged error is obtained based on Eq. (14), by replacing the velocity with bottom shear stress and Uc by $\rho U_c(\omega\nu)^{0.5}$, the maximum bottom shear stress of sinusoidal oscillatory flow in laminar condition. And the error at different phase is the ratio of the difference between the numerical and theoretical bottom shear stresses to $\rho U_c(\omega\nu)^{0.5}$. The maximum error is the maximum of the errors at all phases.

As shown in Table 2, the periodic averaged errors are less than 0.08 when $Re_\delta \leq 550$, and less than 0.3 when $Re_\delta = 800$. When $Re_\delta \geq 1500$, the errors are greater than 0.5. The maximum errors, given in Table 3, are about twice as much as the corresponding periodic averaged errors. Table 4 and Table 5 present the phase proportion in a wave cycle for

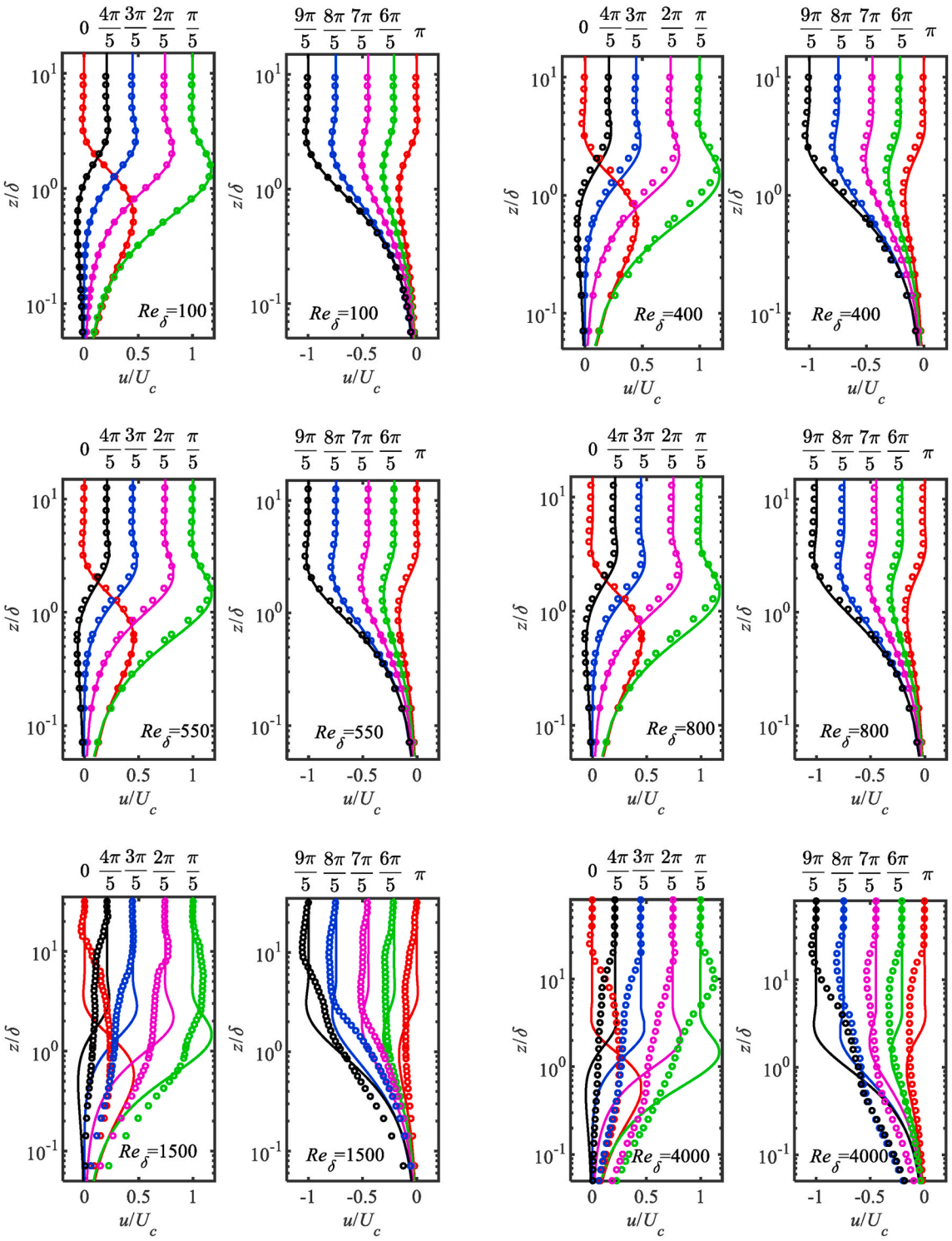

Fig. 14. Comparison between theoretical and numerical velocity profiles for $\beta = 0.8$. The lines and circles show the theoretical results of Eq. (11) and the numerical results, respectively. Different colors represent different phases. (For interpretation of the references to color in this figure legend, the reader is referred to the Web version of this article.)

different error ranges for $\beta = 0.55$ and $\beta = 0.8$, respectively. The distribution of the errors in these two tables further demonstrate that Eq. (13) is able to provide accurate prediction of bottom shear stress when $Re_\delta \leq 550$. When $Re_\delta = 800$, the phase proportion of the errors less than 0.1 is more than 80% for $\beta = 0.8$, but it is about 20% for $\beta = 0.55$. The discrepancies in some phases may be partly due to the development of turbulence, because for the Reynolds number from disturbing laminar to intermittent turbulent flow, the increase of the degree of forward leaning of the wave shape tends to inhibit the development of turbulence to some extent due to less time of fluid acceleration (Scandura et al., 2016). Overall, Eq. (13) is capable of accurately predicting the bottom shear stress in laminar and disturbing laminar flow regimes, and can be roughly extended to the intermittent turbulent flows for $Re_\delta \leq 800$.

4.2.2. *Velocity profile in the boundary layer*

Comparisons of the velocity in the boundary layer at different Rey-

Table 6
Periodic averaged error of velocity at different heights for $\beta = 0.55$

	3/10 δ	5/10 δ	7/10 δ	δ	2δ	4δ	6δ
$Re_\delta = 100$	0.005	0.005	0.006	0.012	0.015	0.011	0.011
$Re_\delta = 400$	0.003	0.008	0.012	0.019	0.017	0.005	0.004
$Re_\delta = 550$	0.003	0.012	0.018	0.026	0.023	0.006	0.004
$Re_\delta = 800$	0.078	0.11	0.12	0.11	0.079	0.077	0.051
$Re_\delta = 1500$	0.16	0.17	0.17	0.14	0.15	0.13	0.099
$Re_\delta = 4000$	0.18	0.14	0.11	0.11	0.20	0.19	0.16

Table 7
Periodic averaged error of velocity at different heights for $\beta = 0.8$

	3/10 δ	5/10 δ	7/10 δ	δ	2δ	4δ	6δ
$Re_\delta = 100$	0.003	0.003	0.004	0.004	0.004	0.006	0.007
$Re_\delta = 400$	0.004	0.014	0.018	0.028	0.016	0.009	0.008
$Re_\delta = 550$	0.005	0.018	0.024	0.029	0.021	0.011	0.009
$Re_\delta = 800$	0.008	0.024	0.032	0.038	0.032	0.027	0.026
$Re_\delta = 1500$	0.13	0.14	0.14	0.11	0.11	0.12	0.091
$Re_\delta = 4000$	0.16	0.15	0.14	0.13	0.18	0.16	0.12

nolds numbers between the numerical and theoretical (obtained by Eq. (11)) results for $\beta = 0.55$ and $\beta = 0.8$ respectively are provided in Figs. 13 and 14. For $Re_\delta \leq 800$, the agreement between the theoretical and numerical results is perfectly good for both cases of $\beta = 0.55$ and $\beta = 0.8$, except for some discrepancy found near the phases of flow reversal in the case of $Re_\delta = 800$ and $\beta = 0.8$. For the cases of $Re_\delta = 1500$ and $Re_\delta = 4000$, the comparison shows distinct differences because of the stronger turbulence.

Similarly, to further perform quantitative analysis on the applicability of Eq. (11), the periodic averaged errors at different vertical positions and the maximum errors at different phases between results calculated by Eq. (11) and the numerical results are calculated. Here, the periodic averaged error is obtained similarly as that by Eq. (14) and the maximum errors at different phases are the maximum ratio of the difference between the numerical and theoretical velocity to U_c in the vertical direction.

As shown in Tables 6 and 7, the periodic averaged errors are lower than 0.03 when $Re_\delta \leq 550$ and around 0.15 when $Re_\delta \geq 1500$. When $Re_\delta = 800$, the errors are lower than 0.04 for $\beta = 0.8$ and lower than 0.12 for $\beta = 0.55$. The maximum errors, given in Tables 8 and 9, are lower than 0.07 when $Re_\delta \leq 550$ and higher than 0.2 for most of phases when $Re_\delta \geq 1500$. When $Re_\delta = 800$, the maximum errors are lower than 0.09 for $\beta = 0.8$ and around 0.2 for $\beta = 0.55$. It is demonstrated that when $Re_\delta = 800$, accurate results can be obtained with the application of Eq. (11) as β increase, and one of the possible reasons is the shortening of acceleration stage. In summary, it is evident that the prediction of the velocity of the boundary layers in laminar and disturbing laminar flow regimes can be performed accurately by Eq. (11) and Eq. (11) can also be roughly applied to the intermittent turbulent flows for $Re_\delta \leq 800$.

5. Conclusions

A novel expression of the near bed orbital velocity beneath forward-leaning waves is worked out. It is a series in which the coefficients are invariable for arbitrarily forward-leaning waves and just depend on the order of expansion. While a few terms for this series are considered, accurate results can be obtained for the degree of forward leaning up to 0.8, covering almost all forward-leaning waves in practice. Comparison with other series expressions evidently demonstrates that the convergence of the present formula can be achieved easily, and this formula can be readily utilized as wave forcing in laboratory experiment and numerical simulation of forward leaning waves.

This new expression is then used as the boundary condition of the governing equation of the boundary layer beneath forward-leaning waves. Consequently, a theoretical solution of the laminar boundary layer beneath forward-leaning waves is derived by solving the governing equation via the method of variable separation. And the velocity and bottom shear stress of the laminar boundary layer beneath forward-leaning waves are readily obtained. Based on these theoretical results, the velocity, the bottom shear stress, the boundary layer thickness, and the phase lag between the free-stream velocity and bottom shear stress are analyzed and discussed. The waveforms of the periodic velocity and bottom shear stress become more asymmetrical as the degree of forward leaning increases. The maximum and minimum bottom shear stresses grow and decrease respectively with the increase of the degree of forward leaning. The phase lag between the free-stream velocity and bottom shear stress decreases obviously from 45° for sinusoidal waves with increasing degree of forward leaning. And the phase lag at the crest is larger than that at the trough because of the acceleration asymmetry. The boundary layer thickness at the wave crest and trough increases and decreases almost linearly with decreasing degree of forward leaning, respectively. Besides, both of them are approaching to the counterpart value of sinusoidal waves when the degree of forward leaning decreases to 0.5. The boundary layer thickness at the wave crest is always smaller than that at the trough because of the shorter time for the increase of velocity from zero to the maximum at the crest than that at the trough. These results may serve as some theoretical references for further

Table 8
Maximum error of velocity at different phases for $\beta = 0.55$

	0	$\frac{\pi}{5}$	$\frac{2\pi}{5}$	$\frac{3\pi}{5}$	$\frac{4\pi}{5}$	π	$\frac{6\pi}{5}$	$\frac{7\pi}{5}$	$\frac{8\pi}{5}$	$\frac{9\pi}{5}$
$Re_\delta = 100$	0.014	0.016	0.027	0.031	0.027	0.023	0.019	0.016	0.019	0.016
$Re_\delta = 400$	0.019	0.018	0.033	0.035	0.029	0.021	0.016	0.022	0.029	0.026
$Re_\delta = 550$	0.026	0.025	0.044	0.046	0.038	0.027	0.021	0.030	0.039	0.036
$Re_\delta = 800$	0.29	0.17	0.084	0.20	0.29	0.21	0.13	0.10	0.20	0.25
$Re_\delta = 1500$	0.24	0.19	0.21	0.24	0.21	0.15	0.12	0.31	0.25	0.19
$Re_\delta = 4000$	0.22	0.21	0.27	0.35	0.26	0.20	0.14	0.26	0.27	0.29

Table 9
Maximum error of velocity at different phases for $\beta = 0.8$

	0	$\frac{\pi}{5}$	$\frac{2\pi}{5}$	$\frac{3\pi}{5}$	$\frac{4\pi}{5}$	π	$\frac{6\pi}{5}$	$\frac{7\pi}{5}$	$\frac{8\pi}{5}$	$\frac{9\pi}{5}$
$Re_\delta = 100$	0.01	0.01	0.01	0.01	0.02	0.01	0.01	0.01	0.01	0.01
$Re_\delta = 400$	0.02	0.05	0.04	0.03	0.02	0.02	0.01	0.01	0.02	0.02
$Re_\delta = 550$	0.02	0.07	0.06	0.04	0.03	0.02	0.02	0.02	0.01	0.02
$Re_\delta = 800$	0.03	0.09	0.08	0.06	0.04	0.04	0.04	0.04	0.04	0.04
$Re_\delta = 1500$	0.22	0.21	0.25	0.18	0.14	0.12	0.09	0.12	0.19	0.17
$Re_\delta = 4000$	0.23	0.40	0.30	0.19	0.15	0.15	0.12	0.13	0.23	0.31

experimental and numerical investigation.

Comparisons with detailed quantitative error analysis of velocity and bottom shear stress between the present theory and the numerical results with increasing Reynolds numbers demonstrate that the theoretical solution is capable of accurately predicting the properties of the boundary layer in laminar and disturbing laminar flow regimes, and can be roughly extended to cover part of the intermittent turbulent flow regimes, although it is obtained for laminar flow.

CRediT authorship contribution statement

Yiqin Xie: Data curation, Writing - original draft, Software, Validation, Visualization. **Jifu Zhou:** Conceptualization, Formal analysis, Methodology, Funding acquisition, Project administration, Supervision, Writing - review & editing. **Xu Wang:** Investigation, Validation, Visualization. **Jinlong Duan:** Writing - review & editing.

Declaration of competing interest

The authors declare that they have no known competing financial interests or personal relationships that could have appeared to influence the work reported in this paper.

Acknowledgments

We very much appreciate the financial support of the National Key R&D Program of China (Grant No. 2017YFC1404202), the National Natural Science Foundation of China (Grant Nos. 11572332 and 51520105014), and the Strategic Priority Research Program of the Chinese Academy of Sciences (Grant Nos. XDB22040203 and XDA22040304).

References

Abreu, T., Silva, P.A., Sancho, F., Temperville, A., 2010. Analytical approximate wave form for asymmetric waves. Coast. Eng. 57 (7), 656–667. https://doi.org/10.1016/j.coastaleng.2010.02.005.

Drake, T.G., Calantoni, J., 2001. Discrete particle model for sheet flow sediment transport in the nearshore. J. Geophys. Res.: Oceans 106 (C9). https://doi.org/10.1029/2000jc000611, 19859–19868.

Elfrink, B., Hanes, D.M., Ruessink, B.G., 2006. Parameterization and simulation of near bed orbital velocities under irregular waves in shallow water. Coast. Eng. 53, 915–927. https://doi.org/10.1016/j.coastaleng.2006.06.002.

Foster, D.L., Guenther, R.A., Holman, R.A., 1999. An analytic solution to the wave bottom boundary layer governing equation under arbitrary wave forcing. Ocean. Eng. 26 (7), 595–623. https://doi.org/10.1016/s0029-8018(98)00016-x.

Hsu, T.J., Hanes, D.M., 2004. Effects of wave shape on sheet flow sediment transport. J. Geophys. Res. 109 https://doi.org/10.1029/2003JC002075. C05025.

Jensen, B.L., Sumer, B.M., Fredsøe, J., 1989. Turbulent oscillatory boundary layer at high Reynolds numbers. J. Fluid Mech. 206, 265–297. https://doi.org/10.1017/S0022112089002302.

Kondo, J., 1956. Operational Method, p. 240pp. Baifukan.

Larson, M., 1996. A closed-form solution for turbulent wave boundary layers. 25th International Conference on Coastal Engineering 3244–3256. https://doi.org/10.1061/9780784402429.251.

Li, Y.J., Chen, J.B., Zhou, J.F., Zhang, Q., 2016. Large eddy simulation of boundary layer flow under cnoidal waves. Acta Mech. Sin. 32 (1), 22–37. https://doi.org/10.1007/s10409-015-0486-6.

Lohmann, I.P., Fredsøe, J., Sumer, B.M., Christensen, E.D., 2006. Large Eddy Simulation of the ventilated wave boundary layer. J. Geophys. Res. 111 (C6) https://doi.org/10.1029/2005jc002946.

Nadaoka, K., Yagi, H., Nihei, Y., Nomoto, K., 1996. Turbulence structure of asymmetrical oscillatory flow. Proc. Coastal Engrg., JSCE 43, 441–445.

Nielsen, P., 2002. Shear stress and sediment transport calculations for swash zone modeling. Coast. Eng. 45, 53–60. https://doi.org/10.1016/S0378-3839(01)00036-9.

Nielsen, P., Callaghan, D.P., 2003. Shear stress and sediment transport calculations for sheet flow under waves. Coast. Eng. 47 (3), 347–354. https://doi.org/10.1016/s0378-3839(02)00141-2.

Ruessink, B.G., van den Berg, T.J.J., van Rijn, L.C., 2009. Modeling sediment transport beneath skewed asymmetric waves above a plane bed. J. Geophys. Res. 114, C11021. https://doi.org/10.1029/2009.JC005416.

Sana, A., Tanaka, H., Yamaji, H., Kawamura, I., 2006. Hydrodynamic behavior of asymmetric oscillatory boundary layers at low Reynolds numbers. J. Hydraul. Eng. 132 (10), 1086–1096. https://doi.org/10.1061/(asce)0733-9429(2006)132:10(1086).

Scandura, P., Faraci, C., Foti, E., 2016. A numerical investigation of acceleration-skewed oscillatory flows. J. Fluid Mech. 808, 576–613. https://doi.org/10.1017/jfm.2016.641.

Silva, P.A., Abreu, T., Sancho, F., Temperville, A., 2007. A sensitivity study of sediment transport rates in accelerated skewed waves. In: Dohmen- Janssen, M., Hulscher, S. (Eds.), Proceedings of the 5th IAHR Symposium on River. : Coastal and Estuarine Morphodynamics. Enschede, The Netherlands, pp. 337–343. https://doi.org/10.1201/NOE0415453639-c43.

Stokes, G.G., 1847. On the theory of oscillatory waves. Trans. Camb. Philos. Soc. 8, 441–455.

Suntoyo, Tanaka, H., Sana, A., 2008. Characteristics of turbulent boundary layers over a rough bed under saw-tooth waves and its application to sediment transport. Coast. Eng. 55 (12), 1102–1112. https://doi.org/10.1016/j.coastaleng.2008.04.007.

Tanaka, H., Sumer, B.M., Lodahl, C., 1998. Theoretical and experiment investigation on laminar boundary layers unders under cnoidal wave motion. Coast Eng. J. 40, 81–98. https://doi.org/10.1142/S0578563498000066.

van der A, D.A., O' Donoghue, T., Davies, A.G., Ribberink, J.S., 2011. Experimental study of turbulent boundary layer in acceleration-skewed oscillatory flow. J. Fluid Mesh 684, 251–283. https://doi.org/10.1017/jfm.2011.300.

Wang, D., Yuan, J., 2020. An experimental study of net sediment transport rate due to acceleration-skewed oscillatory flows over rippled seabeds. Coast. Eng. 155, 103583. https://doi.org/10.1016/j.coastaleng.2019.103583.

Watanabe, A., Sato, S., 2004. A sheet-flow transport rate formula for asymmetric, forward-leaning waves and currents. Proceedings of the 29th International Conference on Coastal Engineering 2, 1703–1714. https://doi.org/10.1142/9789812701916_0136. Lisbon, ASCE.

Yuan, J., Madsen, O.S., 2014. Experimental study of turbulent oscillatory boundary layers in an oscillating water tunnel. Coast. Eng. 89, 63–84. https://doi.org/10.1016/j.coastaleng.2014.03.007.

Zhang, Q., Zhou, J.F., Li, J.C., 2005. Burst detection in turbulent channel flows based on large eddy simulation databases. Sci. China G 48 (4), 469–484.

Glossary

a: Acceleration of free-stream velocity
$a_{k,m}$, A_m: Coefficients of series expansion, k, m is the subscripts
As: Degree of asymmetry
N: Order of series expansion
r: Waveform parameter
Re_δ: Reynolds number
t: Time
T: Wave period
T_{cu}: Time duration for free-stream velocity increasing from zero to the maximum
u: Horizontal velocity
U, $U_{i(ex)}$, $U_{i(ap)}$: Free-stream velocity outside the boundary layer with the subscript i representing time index, and the subscripts (ex) and (ap) denoting the results of Eq. (3) and Eq. (9), respectively
U_c: Velocity amplitudes
z: Vertical coordinate
α: A multiplier
β: Degree of forward leaning
δ: Stokes layer thickness
δ_c: Boundary layer thickness at wave crest
δ_t: Boundary layer thickness at wave trough
ϕ: Phase lag between free-stream velocity and bottom shear stress
ν: Kinematic viscosity of fluid
τ: Shear stress
τ^*: Dimensionless shear stress
τ_0: Bottom shear stress
τ_0^*: Dimensionless bottom shear stress
ω: Angular velocity
ξ: Parameter to describe the acceleration skewness
ζ: A coefficient adjust the degree of forward leaning of velocity